Eur. Phys. J. A (2020) 56:231
https://doi.org/10.1140/epja/s10050-020-00231-8

THE EUROPEAN PHYSICAL JOURNAL A

Review

Photon induced processes: from ultraperipheral to semicentral heavy ion collisions

Wolfgang Schäfer[a]

Institute of Nuclear Physics Polish Academy of Sciences, ul. Radzikowskiego 152, 31-342 Kraków, Poland

Received: 31 May 2020 / Accepted: 23 August 2020 / Published online: 17 September 2020

Communicated by Laura Tolos

Abstract We present an overview of processes induced by the coherent Weizsäcker-Williams (WW) photon cloud in heavy ion collisions. Due to the rather broad energy spectrum of photons a large variety of physics topics can be addressed. At the low-energy side, there are the electromagnetic dissociation processes. We discuss the few-neutron production via giant dipole resonance excitation. A typical high energy photonuclear process that has attracted much attention is the diffractive photoproduction of vector mesons. We review the color dipole approach to coherent and incoherent diffractive photoproduction of J/ψ mesons. Finally we turn to peripheral and semicentral collisions and discuss the role of WW photons in the production of very low-P_T dileptons.

1 Introduction; equivalent photon approximation

Fast moving heavy ions are accompanied by their cloud of Weizsäcker-Williams (WW) photons, which offer the possibility to study a large range of photon-photon processes as well as photonuclear processes ranging from low to high energies [1–3]. The WW photons couple coherently to the whole nucleus, and photon fluxes in an ion are enhanced by the square of the large charge $Z|e|$. For example for the gold and lead ions, $Z = 79, 82$, respectively. While the charge at rest is surrounded by its electric Coulomb field, the field generated by a highly boosted current consists of electric and magnetic fields which are of (almost) the same size and (almost) orthogonal to each other. This corresponds to the situation of a plane-wave electromagnetic field which can be viewed as a flux of (quasireal) photons. If we assume that the charge moves at an impact parameter $\boldsymbol{b}$, with relativistic velocity $\beta \approx 1$, at a boost $\gamma = 1/\sqrt{1-\beta^2} \gg 1$, we can easily obtain the field strength as [4]

$$\boldsymbol{E}(\omega, \boldsymbol{b}) = -i\,\frac{Z\sqrt{4\pi\alpha_{em}}}{2\pi}\,\frac{\boldsymbol{b}}{b^2}\,\frac{\omega b}{\gamma}K_1\Big(\frac{\omega b}{\gamma}\Big). \tag{1}$$

Here K_1 is the modified Bessel function, and ω is the photon energy in the considered frame. We omitted a term $\propto 1/\gamma$, and put $\beta = 1$ wherever possible. This simple result is valid for a point-like charge, it cannot be correct for the finite-size nucleus, for $b < R_A$. The finite size of the nucleus is easily accounted for by using

$$\boldsymbol{E}(\omega, \boldsymbol{b}) = Z\sqrt{4\pi\alpha_{em}}\int \frac{d^2\boldsymbol{q}}{(2\pi)^2}\,\frac{e^{-i\boldsymbol{b}\boldsymbol{q}}\boldsymbol{q}F_{em}(\boldsymbol{q}^2+\omega^2/\gamma^2)}{\boldsymbol{q}^2+\omega^2/\gamma^2}, \tag{2}$$

where $F_{em}(Q^2)$ is the charge form factor of the nucleus, which is essentially a Fourier transform of the charge distribution. For heavy nuclei, such as Au or Pb, the pointlike formula Eq. (1) is an excellent approximation for $b > 20$ fm. For many ultraperipheral processes, where the essential contribution comes from $b \gg R_A$, it is sufficient to simply cut off the region $b < R_A$ in most integrated cross sections. However, especially for the calculation of distributions in invariant mass or transverse momentum of a produced system (see, e.g. [5,6]), the use of a realistic form-factor, such as the one implemented in the STARlight Monte-Carlo [7], is recommended.

The photon flux finally is obtained from the electric field (or more precisely from the Poynting vector $\boldsymbol{S} \propto \boldsymbol{E} \times \boldsymbol{B}$) as

$$N(\omega, \boldsymbol{b}) = \frac{1}{\omega}\frac{1}{\pi}\Big|\boldsymbol{E}(\omega, \boldsymbol{b})\Big|^2. \tag{3}$$

Then, cross sections involving the electromagnetic interaction in the collision of ions A and B, where A serves as the source of the WW photons can be calculated from the γB cross section convoluted with the flux of photons:

$$\sigma(AB) = \int d\omega d^2\boldsymbol{b}\, N(\omega, \boldsymbol{b})\,\sigma(\gamma B; \omega). \tag{4}$$

[a] e-mail: Wolfgang.Schafer@ifj.edu.pl (corresponding author)

The apparent frame dependence of the *energy distribution* of photons, could be easily avoided by using momentum or energy fractions. It is useful to use per-nucleon energies, and hence the corresponding $x = \omega/E_N = \omega/(\gamma m_N)$ with $dx/x = d\omega/\omega$. Then Eq. (4) becomes the standard parton-model expression, with WW photons as partons of the nucleus.

From the plethora of processes which involve WW photons, a few are indicated in Fig. 1. They include pure QED processes, like pair production of dileptons, as well as low-energy nuclear reactions, such as electromagnetic excitation of one of the ions, say into a giant resonance state. From the realm of high-energy nuclear interactions we mention the diffractive coherent and incoherent photoproduction of vector mesons. Also of interest are generic photoabsorption processes with multiparticle production containing for example jets as a probe of nuclear partons.

Electromagnetically induced cross sections can be very large, owing to the long range of the interaction.

Strong interactions are of finite range, and thus require two nuclei to have geometric overlap. Once nuclei do come close enough, though, an interaction happens with probability of one – the defining property of strong interactions indeed. If we want predict a cross section without strong interactions between ions, i.e. without additional production of particles, we need to take the constraint of no additional interaction into account. For example, for the process of coherent diffractive vector meson production, we would use an effective photon flux

$$\sigma(A_1A_2 \to A_1A_2V; s) = \int d\omega N_{A_1}^{\rm eff}(\omega) \times \sigma(\gamma A_2 \to VA_2; 2\omega\sqrt{s}) + (1 \leftrightarrow 2), \quad (5)$$

for which we simply multiplied in impact parameter space by the probability of no interaction between the ions:

$$N^{eff}(\omega) = \int d^2\boldsymbol{b}\, P_{\rm surv}(\boldsymbol{b}) N(\omega, \boldsymbol{b})\,. \quad (6)$$

This probability, in analogy to the absorptive corrections in diffractive production processes [8] is called the *rapidity gap survival probability*, where here a survival against strong interactions is meant. The latter is essentially the square of the elastic (strong-interaction) S-matrix of ions, and amounts in practice to the geometric cutoff [9]:

$$P_{\rm surv}(\boldsymbol{b}) = S_{el}^2(\boldsymbol{b}) = \exp\Big(-\sigma_{NN} T_{A_1A_2}(\boldsymbol{b})\Big) \sim \theta(|\boldsymbol{b}| - (R_1 + R_2)).$$

For a discussion of the accuracy of the last approximation, see e.g. [10] for the case of dilepton production. Notice that the survival probability breaks the factorization of the photon-flux representation of cross sections. The effective flux of Eq. (6) can only be used in reactions involving a single photon exchange. For photon-photon fusion reactions the analogous procedure of including absorptive corrections can be applied to the $\boldsymbol{b}$-space formulation of the cross section, but the result will not involve the flux of Eq. (6) but rather an effective photon-photon luminosity. We finally note, that the size of the photon source controls the maximal photon energy attainable at a certain collision energy, roughly $\omega_{\rm max} \sim \gamma/R_A$. Clearly, WW photons also play a role in proton-proton collisions, where much higher photon energies can be achieved than in nucleus-nucleus collisions, however with a much reduced coupling/intensity. Finally proton-nucleus collisions offer an excellent opportunity to access photoproduction on the proton, exploiting the nucleus as the photon source.

The rest of this paper will be devoted to a biased choice of electromagnetically induced processes to which the author has contributed. We will start from ultraperipheral collisions (UPCs) at high energies. Much additional information on the

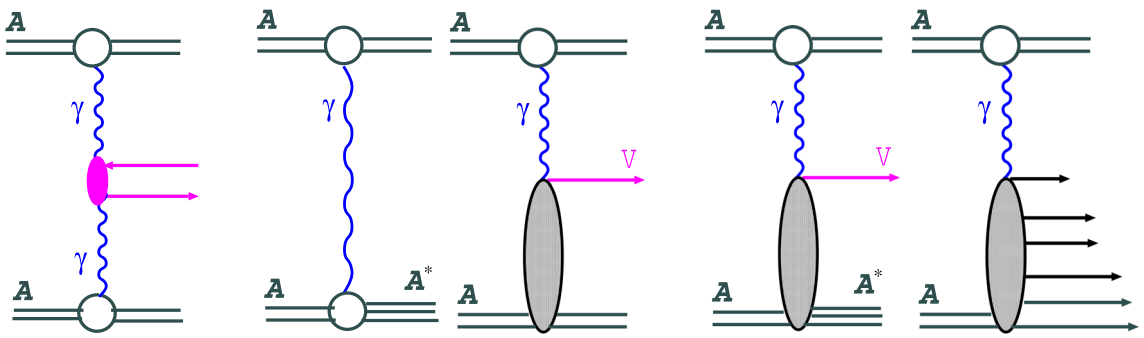

Fig. 1 Some photon induced processes in (ultra-)peripheral heavy ion collisions. From left to right: 1. lepton pair production via $\gamma\gamma$-fusion; 2. electromagnetic excitation of one of the ions, e.g. into a giant dipole resonance; 3. coherent diffractive photoproduction of a vector meson; 4. Incoherent diffractive photoproduction - one of the nuclei breaks up; 5. a generic inelastic photon-nucleus process with multiple particle production in the final state

processes discussed below can be found in the recent review [3].

In Sect. 2 we will discuss the electromagnetic dissociation of nuclei into giant dipole resonances (GDRs), and their contribution to few-neutron production in the nuclear fragmentation region. In Sect. 3 we discuss a class of high-energy photonuclear processes: the coherent and incoherent diffractive photoproduction of J/ψ mesons. We show how in the color dipole approach predictions can be made that generalize the Glauber multiple scattering theory and are based on a color-dipole cross section that describes the diffractive $\gamma p \to J/\psi p$ process. Then, in Sect. 4 we lift the restriction of ultraperipherality and show how fusion of WW photons is the mechanism behind the production of dileptons at very low pair transverse momentum in peripheral to semicentral centrality classes.

2 Electromagnetic excitation of heavy ions

The measurement of ultraperipheral reactions at the high energies of present day colliders (RHIC and LHC) often requires special triggers. The presence of large fluxes of WW photons, sharply peaked at low photon energies, leads to the possibility of electromagnetic excitation of one or both of the ions. Here low-energy excitations, with energies in the nuclear rest frame of $E^* < 50$ MeV play an especially important role. These low-energy excited nuclear heavy systems, close to giant resonance region, decay predominantly via emission/evaporation of few neutrons. Because the energy of the neutrons in the nucleus rest frame is rather small ~ 10 to 20 MeV, in the highly boosted situation of UPCs the neutrons are emitted in very small angular cones around beam directions. Such neutrons can be registered by the so-called zero-degree calorimeters (ZDC's) which are associated with many high-energy detectors, such as e.g. STAR at RHIC and ALICE at LHC.

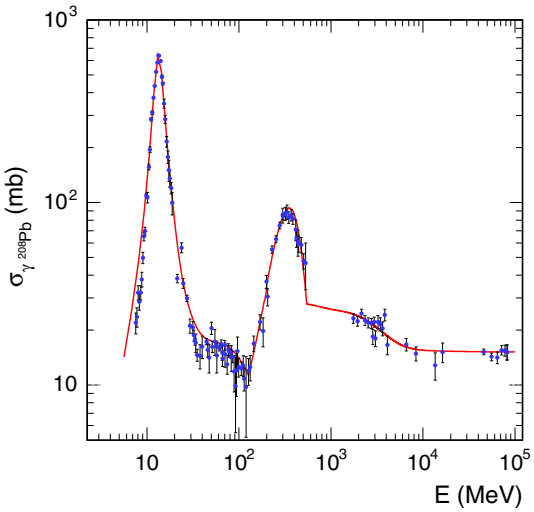

Fig. 2 Photoabsorption cross section on ^{208}Pb

In [11] we developed an approach which combines the description of photoexcitation of nuclei by WW photons and the decay of excited nuclei in the framework of Hauser-Feshbach theory. We calculated topological cross sections with a given number of neutrons in ion-ion collisions from the subprocess $\gamma Pb \to Pb^* + k$ neutrons.

The formalism for the relevant multiphoton exchange processes can be found in [12–14]. The crucial ingredient is the effective number of photons colliding with, say ion # 2:

$$\bar{n}_{A_2}(\boldsymbol{b}) \equiv \int_{E_{\min}}^{\infty} dE\, N_{A_1}(E, \boldsymbol{b}) \sigma_{\rm tot}(\gamma A_2;\, E).$$

As an input we need the total photoabsorption cross section of a given nucleus, see Fig. 2 for the case of ^{208}Pb. The cross section for excitation of one of the ions is dominated by the absorption of a single photon:

$$\begin{aligned}\sigma_{\rm tot}(A_1 A_2 \to A_1 A_2^*;\, E_{\max}) &\approx \int d^2\boldsymbol{b}\, P_{\rm surv}(\boldsymbol{b}) \exp[-\bar{n}_{A_2}(\boldsymbol{b})] \\ &\times \int_{E_{\min}}^{E_{\max}} dE\, N_{A_1}(E, \boldsymbol{b}) \sigma_{\rm tot}(\gamma A_2;\, E). \end{aligned} \tag{7}$$

Here we again encounter the survival probability $P_{\rm surv}(\boldsymbol{b})$ which puts a veto on additional strong interactions between ions.

We are interested mainly in final states that contain a few neutrons, and want to study excitation cross sections as a function of neutron multiplicity. We then need as an input crucial the fractions $f(E, k)$ of final states with k neutrons coming from the decay of an excited nucleus at excitation energy E. To obtain these fractions, we use the Monte-Carlo program GEMINI [15] based on Hauser-Feshbach formalism, which allows us to describe excitation functions of few neutron final states in photoabsorption, see Fig. 3. Then, we can calculate the impact parameter profiles for processes with k evaporated neutrons as:

$$\begin{aligned}\frac{dP_{A_2}^{\rm exc}(\boldsymbol{b}, k)}{dE} &= f(E, k) \cdot \sum_n w_n(\boldsymbol{b}) p_{A_2}^{(n)}(E, \boldsymbol{b}) \\ &\approx f(E, k)\, p_{A_2}^{(1)}(E, \boldsymbol{b}) \bar{n}_{A_2}(\boldsymbol{b}) \exp[-\bar{n}_{A_2}(\boldsymbol{b})], \end{aligned} \tag{8}$$

and, correspondingly:

$$P_{A_2}^{\rm exc}(\boldsymbol{b}, k) = \int_{E_{\min}}^{E_{\max}} dE \frac{dP_{A_2}^{\rm exc}(\boldsymbol{b})}{dE}. \tag{9}$$

The cross section for k-neutron excitation is then

$$\sigma(A_1 A_2 \to A_1(k{\rm N}, X)) = \int d^2\boldsymbol{b}\, P_{\rm surv}(\boldsymbol{b})\, P_{A_2}^{\rm exc}(\boldsymbol{b}, k). \tag{10}$$

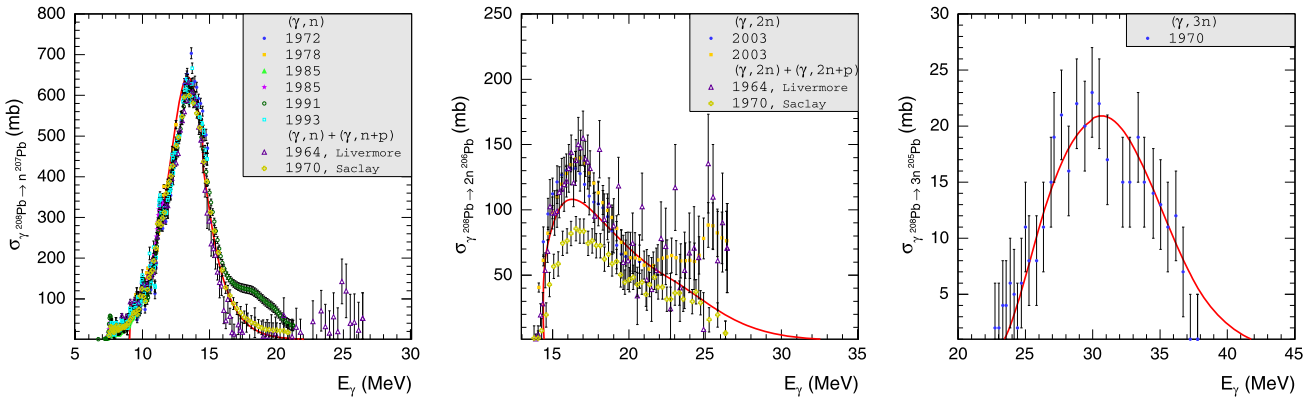

Fig. 3 From left to right: Excitation functions for the $\gamma\,^{208}\mathrm{Pb} \rightarrow \mathrm{n}^{207}\mathrm{Pb}$, $\gamma\,^{208}\mathrm{Pb} \rightarrow 2\mathrm{n}^{206}\mathrm{Pb}$, and $\gamma\,^{208}\mathrm{Pb} \rightarrow 3\mathrm{n}^{205}\mathrm{Pb}$ reactions

Of course we are confined to low-neutron multiplicities, as final states of large number of neutron (k) can be produced by processes in the energy region $E > E_{\max}$ which we do not model so far. Analogously, the mutual excitation cross sections with m and k neutrons in the debris of nucleus A_1, A_2, respectively, is given by

$$\sigma(A_1A_2 \rightarrow (m\mathrm{N}, X)(k\mathrm{N}, Y)) = \int d^2\boldsymbol{b}\, P_{\mathrm{surv}}(\boldsymbol{b}) \times P^{\mathrm{exc}}_{A_1}(\boldsymbol{b}, m)\, P^{\mathrm{exc}}_{A_2}(\boldsymbol{b}, k). \quad (11)$$

In Fig. 4 we show the total cross section for electromagnetic excitation as a function of $\sqrt{s_{NN}}$ as well as the partial cross sections into one and two-neutron final states. We see that at LHC the few-neutron cross section via electromagnetic dissociation (EMD) amounts to $\sim$ 200 barn, much larger than the total lead-lead hadronic cross section. It should be noted that we concentrate only on the neutrons evaporated from the electromagnetically excited nuclei. We do not account for neutrons from other hadronic processes, like the intranuclear cascading (see for example [13] and references therein). By imposing the "gap survival factor", we also discard the mutual excitation of nuclei by strong interactions.

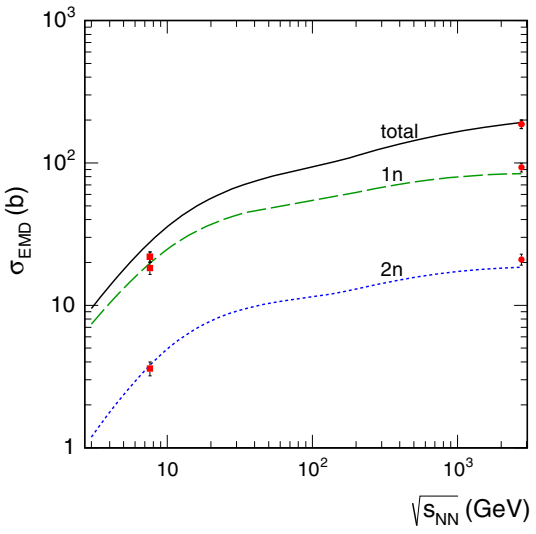

Fig. 4 Single EMD cross sections as the function of $\sqrt{s_{NN}}$. Data are from SPS and LHC (ALICE)

3 Coherent and incoherent diffractive photoproduction of J/ψ

Diffractive dissociation processes are much studied phenomena in hadronic and photon-induced interactions (see e.g. [16] for an introduction). Here one or both of the colliding particles dissociates or is excited into a resonance. The mass of the produced system is much smaller than the cm-energy of the collision. Reaction products are produced in the fragmentation region of beam or target respectively, the products of both being separated by a large gap in rapidity. Only vacuum quantum numbers are exchanged in the cross channel, and the transverse momentum transfer distribution exhibits a characteristic "diffraction cone".

Let us concentrate on the case of diffractive dissociation of a photon on a nuclear target. The prominent final states are vector mesons, being carriers of photon quantum numbers J^{PC}. One generally distinguishes between coherent (or exclusive) diffraction, where the nucleus stays in its ground state, and incoherent diffraction, which includes the excitation of the target nucleus into an excited state, or dominantly, the breakup of the nucleus (see Fig. 5). An important qualifier is, that here we restrict ourselves to diffractive processes in which no new particles are produced in the nuclear fragmentation region.

Much attention has been paid in the past on diffractive photo- and electroproduction of vector mesons on the proton. A large body of data has been accumulated in particular at the DESY-HERA facility. For a review of experimental data and of the theoretical approaches, see [17].

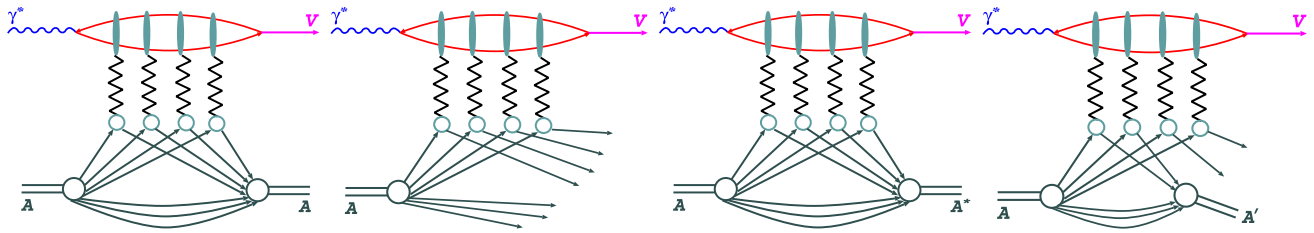

Fig. 5 Diffractive (virtual) photoproduction of a vector meson on a nuclear target. Shown are sample diagrams of a multiple scattering expansion of a color dipole. The four diagrams depict different possible final states. From left to right: (1) coherent diffraction with the outgoing nucleus in the ground state; (2) incoherent diffraction with breakup of the nucleus, (3) diffractive excitation of the nucleus into an excited state, (4) incoherent diffraction including a heavy nuclear fragment in the final state

Here we will review the color dipole approach to the coherent and incoherent photoproduction of J/ψ as used recently by us in [18,19]. Motivated by the recent experiments [20–25], and following the pioneering work of Klein and Nystrand [26], and Goncalves and Machado [27] in the color dipole approach, the exclusive production of J/ψ in ultra-peripheral heavy-ion collisions has been investigated using a number of different theoretical approaches. We will give a brief overview of recent works brief in Sect. 3.4. For more references, see also the review [28].

3.1 Diffractive photoproduction on the free nucleon target

The diffractive production of a vector meson V of mass M_V at high energies, is characterized by a coherence length $l_c = 2\omega/M_V^2$ much larger than the size of the proton $l_c \gg R_N$, where ω is the photon energy in the proton rest frame. In such a situation the V photoproduction can be described as an elastic scattering of a $q\bar{q}$ color dipole of size r, which is conserved during the interaction [29,30]. The $\gamma \to q\bar{q}$ transition and projection of the $q\bar{q}$ pair on the bound state are encoded in the relevant light-cone wave functions. Besides the dipole size, they depend also on the fraction z of the photon's light-front momentum carried by the quark. This results in the (imaginary part of the) forward amplitude of the form

$$\Im m A(\gamma^*(Q^2)p \to Vp; W, t=0) = \int_0^1 dz \int d^2\boldsymbol{r}\, \psi_V(z,\boldsymbol{r})\, \psi_{\gamma^*}(z,\boldsymbol{r},Q^2)\, \sigma(x,\boldsymbol{r}) \qquad (12)$$

Here the dipole cross section is related to the unintegrated gluon distribution of the proton through:

$$\sigma(x,\boldsymbol{r}) = \frac{4\pi}{3}\alpha_S \int \frac{d^2\boldsymbol{\kappa}}{\boldsymbol{\kappa}^4}\mathcal{F}(x,\boldsymbol{\kappa}^2)\Big[1-e^{i\boldsymbol{\kappa}\boldsymbol{r}}\Big].$$

The energy dependence of the amplitude is encoded in its dependence on $x = (Q^2+M_V^2)/W^2$, where W is the $\gamma^* p$-cms energy. The dipole factorization of Eq. (12) captures the salient features of a rich phenomenology of diffractive VM production. In particular it allows one to model the transition from soft interactions of large dipoles, to the perturbative QCD (pQCD) dominated dynamics of small dipoles. The dipole size probed in the VM production is [17,31]

$$r \sim r_S \approx \frac{6}{\sqrt{Q^2+M_V^2}}, \qquad (13)$$

which offers two handles to control the dipole size: virtuality of the photon and mass of the quark constituent of the meson. This leaves heavy mesons as probes of pQCD dynamics in the case of photoproduction.

In the small-dipole limit of the dipole cross section, one can identify the unintegrated gluon distribution as

$$\mathcal{F}(x,\boldsymbol{\kappa}^2) = \frac{\partial x g(x,\boldsymbol{\kappa}^2)}{\partial \log(\boldsymbol{\kappa}^2)}. \qquad (14)$$

Then, the proportionality of the hard amplitude to the gluon distribution in the proton is put in evidence:

$$\sigma(x,r) = \frac{\pi^2}{3} r^2 \alpha_S(q^2) x g(x,q^2)\,,\ q^2 \approx \frac{10}{r^2}.$$

It is often assumed that this relation can be simply carried over to the case of the nuclear target, this being an important motivation behind the studies of diffractive J/ψ's. However, as will become clear below, in the nuclear case multiple scatterings of the dipole have to be taken into account. These have no simple interpretation in terms of the modification of the nuclear collinear glue.

Let us give a few more details on our calculation of diffractive J/ψ production. The overlap of wave functions has the form [32]

$$\psi_V^*(z,\boldsymbol{r})\psi_\gamma(z,\boldsymbol{r}) = \frac{e_Q\sqrt{4\pi\alpha_{\rm em}}N_c}{4\pi^2 z(1-z)}\Big\{m_Q^2 K_0(m_Q r)\psi(z,r) - [z^2+(1-z)^2]m_Q K_1(m_Q r)\frac{\partial\psi(z,r)}{\partial r}\Big\},$$

and we have used parameters determined in Ref. [33], see [18,19] for further details. There are two more corrections which need to be taken into account. Firstly, the real part of

the amplitude, which can be restored from analyticity

$$\sigma(x,r) \to (1 - i\rho(x))\sigma(x,r)\,,\ \rho(x) = \tan\left(\frac{\pi \Delta_{I\!P}}{2}\right), \quad (15)$$

It is related to the energy dependence of the amplitude through the effective intercept

$$\Delta_{I\!P} = \frac{\partial \log\left(\langle V|\sigma(x,r)|\gamma\rangle\right)}{\partial \log(1/x)}. \quad (16)$$

We also neglected the finite longitudinal momentum transfer. Taking the latter into account, the amplitude will no longer be related to the gluon density of the target, but to a generalized, or skewed parton density. At low values of x, one can however use ordinary "diagonal" partons and multiply the latter by a factor:

$$R_{\rm skewed} = \frac{2^{2\Delta_{I\!P}+3}}{\sqrt{\pi}} \cdot \frac{\Gamma(\Delta_{I\!P} + 5/2)}{\Gamma(\Delta_{I\!P} + 4)}\,, \quad (17)$$

which again is controlled by the effective intercept $\Delta_{I\!P}$. The diffractive cross section then receives a correction factor

$$K = (1 + \rho^2(x)) \cdot R^2_{\rm skewed}. \quad (18)$$

For the dipole cross section a large amount of models are available. We use among others a recent fit [34] to combined HERA structure function data, which uses the ansatz

$$\sigma(x,r) = \sigma_0\left(1 - \exp\left[-\frac{\pi^2 r^2 \alpha_s(\mu^2) x g(x,\mu^2)}{3\sigma_0}\right]\right)\,, \quad (19)$$

with

$$\mu^2 = C/r^2 + \mu_0^2. \quad (20)$$

We have also tried alternative parametrizations of Refs. [35–38].

In Fig. 7 we compare our results to the available data on diffractive J/ψ photoproduction. A good agreement is obtained in the energy range of $W = 30$–200 GeV, in which data predominantly originate from HERA. We will see that it is this range of energy which is most important for the calculations in UPCs.

3.2 Coherent and incoherent diffractive photoproduction on the nuclear target

Let us briefly recapitulate the color dipole approach to coherent photoproduction on the nucleus, which is a variant of Glauber-Gribov multiple scattering theory. It sums up multiple scatterings of a color-dipole within the nucleus, see a typical diagram in Fig. 5.

A general amplitude, at finite momentum transfer, for the process $\gamma A_i \to V A_f$ can be written as

$$\mathcal{A}(\gamma^* A_i \to V A_f^*; W, \Delta) = 2i \int d^2\boldsymbol{B} \exp[-i\boldsymbol{\Delta B}]$$

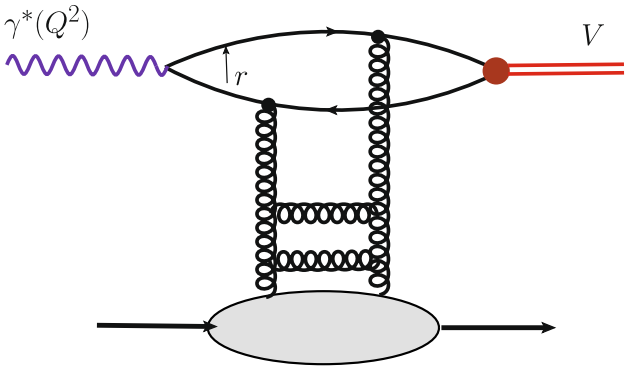

Fig. 6 A Feynman diagram for the $\gamma^* p \to V p$ process. The photon splits into a $q\bar{q}$ color dipole of size $\boldsymbol{r}$. The interaction is described by the (unintegrated) gluon density of the proton

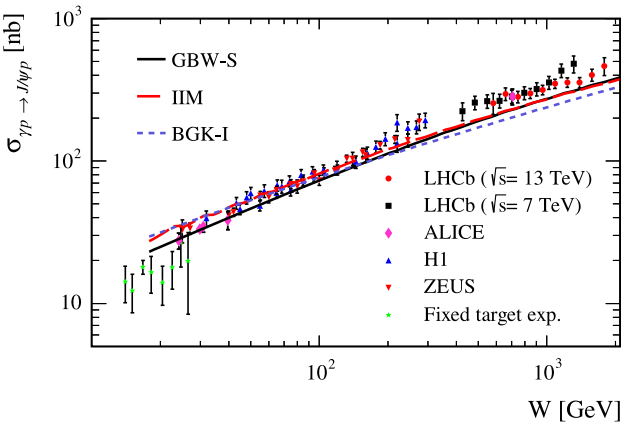

Fig. 7 Total cross section for the exclusive photoproduction $\gamma p \to J/\psi p$ as a function of γp-cms energy W. The results for three different dipole cross-sections are shown. See Ref. [19] for more details on the data points

$$\times \langle V|\langle A_f^*|\hat{\Gamma}(\boldsymbol{b}_+, \boldsymbol{b}_-)|A_i\rangle|\gamma\rangle$$
$$= 2i \int d^2\boldsymbol{B} \exp[-i\boldsymbol{\Delta B}]$$
$$\times \int_0^1 dz \int d^2\boldsymbol{r} \psi_V^*(z,\boldsymbol{r})\psi_\gamma(z,\boldsymbol{r})$$
$$\times \langle A_f^*|\hat{\Gamma}(\boldsymbol{B} - (1-z)\boldsymbol{r}, \boldsymbol{B} + z\boldsymbol{r})|A_i\rangle. \quad (21)$$

We introduced the notation:

$$\boldsymbol{r} = \boldsymbol{b}_+ - \boldsymbol{b}_-,\ \boldsymbol{b} = (\boldsymbol{b}_+ + \boldsymbol{b}_-)/2\,,$$
$$\boldsymbol{B} = z\boldsymbol{b}_+ + (1-z)\boldsymbol{b}_- = \boldsymbol{b} - (1-2z)\frac{\boldsymbol{r}}{2} \quad (22)$$

The main task is now the evaluation of the nuclear averages of the dipole scattering amplitude (or profile function in the standard terminology of Glauber-theory).

Let us start with the case of coherent diffraction, $A_i = A_f$. The diffractive amplitude is now

$$\mathcal{A}(\gamma^* A_i \to V A_i; W, \Delta) = 2i \int d^2\boldsymbol{b} \exp[-i\boldsymbol{b\Delta}]$$

$$\times \int d^2\boldsymbol{r}\rho_{V\gamma}(\boldsymbol{r},\boldsymbol{\Delta})\langle A_i|\hat{\Gamma}(\boldsymbol{b}+\frac{\boldsymbol{r}}{2},\boldsymbol{b}-\frac{\boldsymbol{r}}{2})|A_i\rangle\,, \tag{23}$$

with the overlap of photon and VM wave functions

$$\rho_{V\gamma}(\boldsymbol{r},\boldsymbol{\Delta}) = \int_0^1 dz \exp[i(1-2z)\frac{\boldsymbol{r}\boldsymbol{\Delta}}{2}]\psi_V^*(z,\boldsymbol{r})\psi_\gamma(z,\boldsymbol{r}).$$

The z-dependent phase factor is a relativistic kinematic effect, which is not always accounted for correctly in the literature. However for heavy vector mesons within the presently used overlap of light-front wave functions, which derives from the γ_μ-vertex of the $c\bar{c}\to J/\psi$ transition, it is beyond our accuracy and can be neglected.

One can then use the standard techniques of Glauber theory. First one writes the nuclear profile function as a multiple scattering expansion over free nucleon profile functions

$$\hat{\Gamma}(\boldsymbol{b}_+,\boldsymbol{b}_-) = 1-\prod_{i=1}^{A}[1-\hat{\Gamma}_{N_i}(\boldsymbol{b}_+-\boldsymbol{c}_i,\boldsymbol{b}_--\boldsymbol{c}_i)]\,,$$

The nuclear averages of free-nucleon amplitudes are standard:

$$\begin{aligned} M(\boldsymbol{b}_+,\boldsymbol{b}_-) &= \int d^2\boldsymbol{c}T_A(\boldsymbol{c})\Gamma_N(\boldsymbol{b}_+-\boldsymbol{c},\boldsymbol{b}_--\boldsymbol{c}) \\ &\approx \frac{1}{2}\sigma(\boldsymbol{r})T_A(\boldsymbol{b})\,, \end{aligned}$$

and within the common dilute gas approximation of uncorrelated nucleons they only involve the optical density $T_A(\boldsymbol{b})$ of a nucleus. Then, in the large-A limit one obtains the well-known exponentiation

$$\begin{aligned} \langle A_i|\hat{\Gamma}(\boldsymbol{b}+\frac{\boldsymbol{r}}{2},\boldsymbol{b}-\frac{\boldsymbol{r}}{2})|A_i\rangle &= 1-\Big[1-\frac{1}{A}M(\boldsymbol{b}_+,\boldsymbol{b}_-)\Big]^A \\ &\approx 1-\exp[-\frac{1}{2}\sigma(\boldsymbol{r})T_A(\boldsymbol{b})]. \end{aligned} \tag{24}$$

Here we have neglected the real part of the amplitude, which can be however accounted for in a straightforward way, see [19]. The differential cross section is obtained from the amplitude according to

$$\frac{d\sigma_{\rm coh}}{d\boldsymbol{\Delta}^2} = \frac{1}{16\pi}\Big|\mathcal{A}(\gamma^* A_i\to VA_i^*;W,\Delta)\Big|^2. \tag{25}$$

In the numerical calculation, we also account for the longitudinal momentum transfer by including a nuclear form factor. This accounts for the suppression of the cross section, when the coherency condition $l_c \gg R_A$ is not fulfilled, see the discussion in [30].

Let us now come to the incoherent diffraction. The evaluation of the nuclear amplitude for a concrete final state is a difficult task, it is only the ground-state average of the profile-function operator which can be evaluated in a straightforward way. One can however address the cross section

$$\frac{d\sigma_{\rm incoh}}{d\boldsymbol{\Delta}^2} = \sum_{A_f\neq A}\frac{d\sigma(\gamma A_i\to VA_f^*)}{d\boldsymbol{\Delta}^2}\,, \tag{26}$$

where the sum goes over all possible nuclear final states and continuum multi-nucleon states, such that the completeness relation

$$\sum_{A\neq A_f}|A_f\rangle\langle A_f| = 1-|A\rangle\langle A|, \tag{27}$$

can be employed. The incoherent cross section now is written as

$$\begin{aligned} \frac{d\sigma_{\rm incoh}}{d\boldsymbol{\Delta}^2} &= \frac{1}{4\pi}\int d^2\boldsymbol{r}d^2\boldsymbol{r}'\rho_{V\gamma}^*(\boldsymbol{r}',\boldsymbol{\Delta})\rho_{V\gamma}(\boldsymbol{r},\boldsymbol{\Delta}) \\ &\quad\times\Sigma_{\rm incoh}(\boldsymbol{r},\boldsymbol{r}',\boldsymbol{\Delta})\,, \end{aligned} \tag{28}$$

with

$$\begin{aligned} \Sigma_{\rm incoh}(\boldsymbol{r},\boldsymbol{r}',\boldsymbol{\Delta}) &= \int d^2\boldsymbol{b}d^2\boldsymbol{b}'\exp[-i\boldsymbol{\Delta}(\boldsymbol{b}-\boldsymbol{b}')] \\ &\quad\times\mathcal{C}\Big(\boldsymbol{b}'+\frac{\boldsymbol{r}'}{2},\boldsymbol{b}'-\frac{\boldsymbol{r}'}{2};\boldsymbol{b}+\frac{\boldsymbol{r}}{2},\boldsymbol{b}-\frac{\boldsymbol{r}}{2}\Big). \end{aligned} \tag{29}$$

Here the function

$$\begin{aligned} \mathcal{C}(\boldsymbol{b}'_+,\boldsymbol{b}'_-;\boldsymbol{b}_+,\boldsymbol{b}_-) &= \langle A|\hat{\Gamma}^\dagger(\boldsymbol{b}'_+,\boldsymbol{b}'_-)\hat{\Gamma}(\boldsymbol{b}_+,\boldsymbol{b}_-)|A\rangle \\ &\quad-\langle A|\hat{\Gamma}(\boldsymbol{b}'_+,\boldsymbol{b}'_-)|A\rangle^*\langle A|\hat{\Gamma}(\boldsymbol{b}_+,\boldsymbol{b}_-)|A\rangle \end{aligned}$$

indeed contains only the ground-state nuclear averages, as we required. The complicated multiple convolution structure of Eqs. (28, 29) can be simplified in two limits. The first one is the one of large momentum transfers $\Delta^2 R_A^2 \gg 1$. In this case one can follow the arguments of Glauber and Matthiae, and derive a multiple scattering expansion

$$\begin{aligned} \frac{d\sigma_{\rm incoh}}{d\boldsymbol{\Delta}^2} &= \sum_n\frac{d\sigma^{(n)}}{d\boldsymbol{\Delta}^2} \\ &= \frac{1}{16\pi}\sum_n w_n(\boldsymbol{\Delta})\int d^2\boldsymbol{b}T_A^n(\boldsymbol{b})|I_n(x,\boldsymbol{b})|^2. \end{aligned}$$

If we assume, that the single scattering on a free nucleon within the diffraction cone has a $\boldsymbol{\Delta}^2$ dependence $\propto \exp[-\frac{1}{2}B\boldsymbol{\Delta}^2]$, we can obtain for the n-fold scattering a $\boldsymbol{\Delta}^2$ dependence according to

$$w_n(\boldsymbol{\Delta}) = \frac{1}{n\cdot n!}\cdot\Big(\frac{1}{16\pi B}\Big)^{n-1}\cdot\exp\Big(-\frac{B}{n}\boldsymbol{\Delta}^2\Big).$$

The functions

$$\begin{aligned} I_n(x,\boldsymbol{b}) &= \langle V|\,\sigma^n(x,r)\exp[-\frac{1}{2}\sigma(x,r)T_A(\boldsymbol{b})]|\gamma\rangle \\ &= \int_0^1 dz\int d^2\boldsymbol{r}\,\psi_V^*(z,\boldsymbol{r})\psi_\gamma(z,\boldsymbol{r}) \\ &\quad\times\sigma^n(x,r)\underbrace{\exp[-\frac{1}{2}\sigma(x,r)T_A(\boldsymbol{b})]}_{\text{nuclear absorption}}\,. \end{aligned}$$

control the weight of the n-fold scattering contribution. Notice that there is a nontrivial interplay between the incoherent addition of n-fold scatterings, and the presence of a coherent intranuclear absorption of the dipole amplitude.

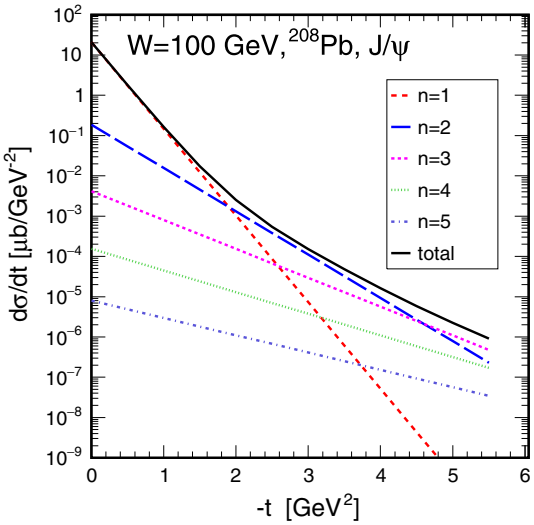

Fig. 8 Incoherent diffractive cross section for $\gamma A \to J/\psi X$ for $A = ^{208}$ Pb at $W = 100$ GeV. We show the contributions from 1 to 5 scatterings. Here a BGK-type dipole cross section was used

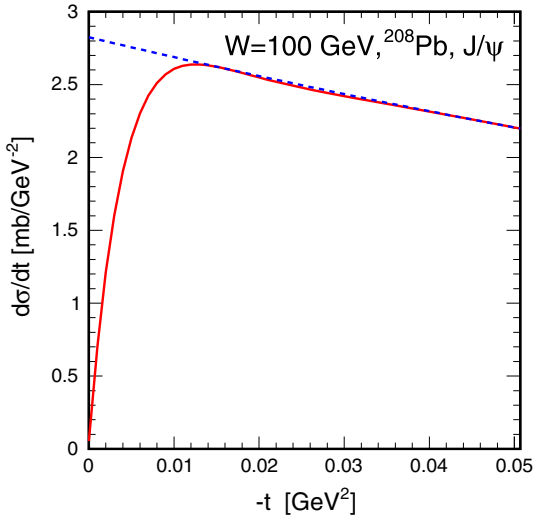

Fig. 9 The incoherent cross section in the very low-t region. The solid line shows the forward dip, while the dashed line is the single scattering term of the large-t limit. A BGK-type dipole cross section was used

In Fig. 8 we show as an example the incoherent diffractive photoproduction cross section for the $\gamma\, ^{208}Pb \to J/\psi\, X$ reaction at a γPb-cms energy of $W = 100$ GeV as a function of $t \approx -\boldsymbol{\Delta}^2$. We show the contributions of up to 5 rescatterings. The higher the number of rescatterings the broader the distribution. We see that the integrated cross section will be dominated by the $n = 1$ scattering.

The second interesting limit is the one of very small momentum transfer $\boldsymbol{\Delta}^2 R_A^2 \ll 1$. In this case one would rather use the exact expression for the single-scattering term:

$$\frac{d\sigma_{\rm incoh}}{d\boldsymbol{\Delta}^2} = \frac{1}{16\pi}\Big\{w_1(\boldsymbol{\Delta}) \int d^2\boldsymbol{b} T_A(\boldsymbol{b})|I_1(x,\boldsymbol{b})|^2 - \underbrace{\frac{1}{A}\Big|\int d^2\boldsymbol{b}\exp[-i\boldsymbol{\Delta b}]T_A(\boldsymbol{b})I_1(x,\boldsymbol{b})\Big|^2}_{\text{vanishes for } \boldsymbol{\Delta}^2 R_A^2 \gg 1}\Big\}.$$

Notice that at large $\boldsymbol{\Delta}^2$ the subtraction term, which induces a dip in the forward region vanishes and the single-scattering term of Eq. (30) is obtained. The very fast convergence to the large $\boldsymbol{\Delta}^2$-limit is evident from Fig. 9. In the absence of intranuclear absorption, one would obtain a standard expression for weak scatterers:

$$\frac{d\sigma_{\rm incoh}}{d\boldsymbol{\Delta}^2} = A \cdot \frac{d\sigma(\gamma N \to VN)}{d\boldsymbol{\Delta}^2}\Big|_{\boldsymbol{\Delta}^2=0} \cdot \Big\{1 - \mathcal{F}_A^2(\boldsymbol{\Delta}^2)\Big\},$$

where $\mathcal{F}_A(\boldsymbol{\Delta}^2)$ is the one-body form factor of the nucleus, normalized as $\mathcal{F}_A(0) = 1$. As we have seen, the incoherent cross section is dominated by the absorption-corrected single scattering term. How large is the effect of intranuclear absorption? This effect is quantified by the ratio

$$R_{\rm incoh}(x) \equiv \frac{d\sigma_{\rm incoh}/d\boldsymbol{\Delta}^2}{A \cdot d\sigma(\gamma N \to VN)/d\boldsymbol{\Delta}^2}$$

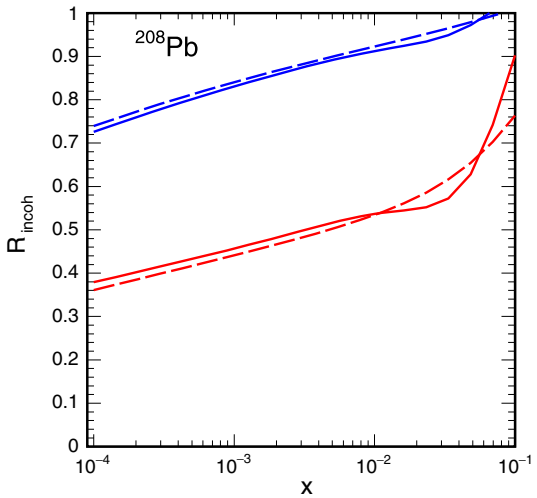

Fig. 10 The nuclear suppression ratio for $\gamma A \to VX$ on lead as a function of $x = m_V^2/W^2$ for $V = \Upsilon$ (upper lines) and $V = J/\psi$ (lower lines). The dashed and solid lines refer to different choices of the free-nucleon color dipole cross section

$$= \frac{\int d^2\boldsymbol{b} T_A(\boldsymbol{b})\Big|\langle V|\sigma(x,r)\exp[-\frac{1}{2}\sigma(x,r)T_A(\boldsymbol{b})]|\gamma\rangle\Big|^2}{A\cdot\Big|\langle V|\sigma(x,r)|\gamma\rangle\Big|^2},$$

which is shown in Fig. 10. We show the results for J/ψ mesons and for the $b\bar{b}$-state Υ. As expected, the smaller dipole sizes relevant in the Υ-case lead to a smaller intranuclear absorption (cf. "color transparency"). Intranuclear absorption for J/ψ is not negligible, and for $x < 0.01$ the dependence on the input dipole cross section is rather small.

Table 1 Subenergies $W_\pm$ and Bjorken-x values $x_\pm$ for $\sqrt{s_{NN}} = 2.76$ TeV for a given rapidity y. Also shown are photon fluxes $n(\omega_\pm)$

$\sqrt{s_{NN}} = 2.76$ TeV						
y	W_+[GeV]	W_-[GeV]	x_+	x_-	$n(\omega_+)$	$n(\omega_-)$
0.0	92.5	92.5	1.12×10^{-3}	1.12×10^{-3}	69.4	69.4
1.0	152	56.1	4.13×10^{-4}	3.05×10^{-3}	39.5	100
2.0	251	34.0	1.52×10^{-4}	8.29×10^{-3}	14.5	132
3.0	414	20.6	5.59×10^{-5}	2.25×10^{-2}	1.68	163
3.8	618	13.8	2.51×10^{-5}	5.02×10^{-2}	0.03	188

3.3 Coherent and incoherent diffractive photoproduction of J/ψ in UPCs

We now come to the coherent photoproduction in UPCs. There are two amplitudes, see Fig. 11 to be added coherently, because each of the ions can be the photon source. The interference between these amplitudes is concentrated at very small transverse momenta [26,39]. It introduces the azimuthal correlation between the outgoing ions, and in the absence of absorptive corrections it would vanish after the angular integration [39]. In our calculation of the rapidity distribution we neglect the interference term, and write

$$\frac{d\sigma(AA \to AAJ/\psi; \sqrt{s_{NN}})}{dy} = n(\omega_+)\sigma(\gamma A \to J/\psi A; W_+) + n(\omega_-)\sigma(\gamma A \to J/\psi A; W_-). \quad (30)$$

Here the WW fluxes are integrated over impact parameter space and include the gap survival factor:

$$n(\omega) = \int d^2\boldsymbol{b} P_{\rm surv}(\boldsymbol{b})\omega N(\omega, \boldsymbol{b}). \quad (31)$$

The two terms in Eq. (30) correspond to the contributions where the left-moving ion serves as the photon source and the right-moving one as the target and vice-versa. The photon energies corresponding to the two contributions are $\omega_\pm = m_V \exp[\pm y]/2$, and the corresponding cm-energies for the $\gamma A \to J/\psi A$ subprocesses are $W_\pm = 2\sqrt{s_{NN}}\omega_\pm$.

For a better understanding of the relevant kinematics, we show in Table 1 the values of $W_\pm$, the associated Bjorken-x values $x_\pm$ as well as photon fluxes $n(\omega_\pm)$ for the example of $\sqrt{s_{NN}} = 2.76$ TeV. At midrapidity of course $W_\pm$ coincide, and we are always well in the energy range that has been explored at HERA for the free nucleon target. Notice, that at larger rapidities it is always the *low-energy* reaction which tends to dominate. This is due to the rather quick drop of the nuclear photon fluxes at high photon energies and the rather modest rise of the nuclear photoproduction cross section.

We show our results for two energies, $\sqrt{s_{NN}} = 2.76$ TeV and 5.02 TeV in Fig. 12. Also shown are data taken by ALICE, CMS and LHCb. We find a good agreement with experiment, except for the midrapidity ALICE result at

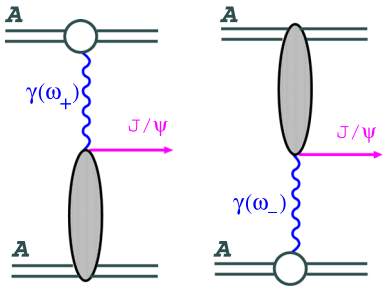

Fig. 11 The two amplitudes for coherent J/ψ production in UPCs

$\sqrt{s_{NN}} = 2.76$ TeV. We therefore suspect that at energies $W \sim 100$ GeV additional effects, such as explicit $c\bar{c}g$-states must be taken into account.

In Fig. 13 we show our result for the incoherent diffractive production of J/ψ at $\sqrt{s_{NN}} = 2.76$ TeV A reasonable agreement with ALICE data is obtained after accounting for the K-factor of Eq. (18).

3.4 A very brief overview of other approaches

Here we give a brief overview of recent works on diffractive J/ψ, and vector meson production in general, in ultraperipheral heavy ion collisions. This however is not a complete review of the available literature, nor can we, due to space limitations, provide extensive discussions of the merits and shortcomings of different approaches. For applications of the color dipole approach to UPCs, some of them extending to light vector mesons and excited states, we refer the reader to [40–52]. The momentum space formulation, $k_\perp$-factorization, which is equivalent to the dipole approach was used in [53], where also $q\bar{q}g$-states were included. A different formulation of Glauber-Gribov theory is used in [54,55]. Other nonperturbative approaches to diffractive vector meson production are put forward in [56,57].

Many of the details of the color-dipole approach have been taken under scrutiny, especially different approaches to the light-front wave functions of the vector meson have been explored in Refs. [47,58–60]. In particular, Krelina et al. [58–60] point to the spurious D-wave component present in the γ_μ-vertex used in the spinorial structure of the vector

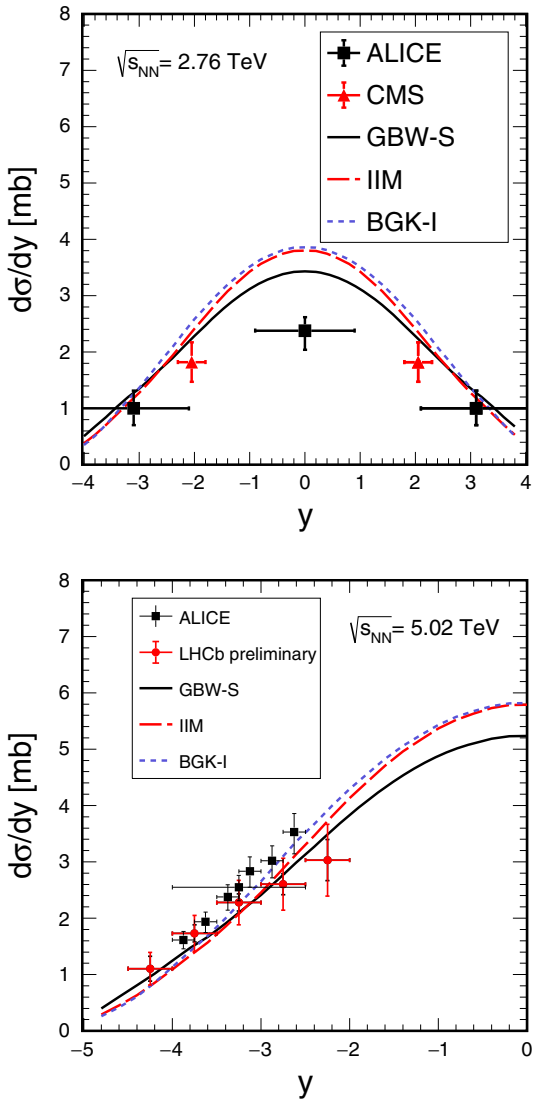

Fig. 12 Upper panel: rapidity dependent cross section $d\sigma/dy$ for exclusive production of J/ψ in ^{208}Pb^{208}Pb-collisions at per-nucleon cms energy $\sqrt{s_{NN}} = 2.76$ TeV. The data are from ALICE [20,22] and CMS [23]. Lower panel: the same for $\sqrt{s_{NN}} = 5.02$ TeV. Shown are the recent ALICE data [25] as well as preliminary data from LHCb [24] (the latter mirrored to the negative rapidity axis)

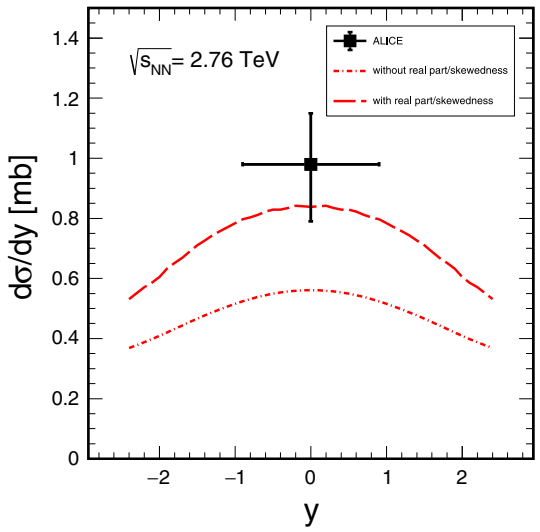

Fig. 13 Rapidity dependent cross section $d\sigma/dy$ for incoherent diffractive production of J/ψ in ^{208}Pb^{208}Pb-collisions at per-nucleon cms energy $\sqrt{s_{NN}} = 2.76$ TeV. We show the results with and without the K-factor, Eq. (18). The ALICE data point is from Ref. [22]

meson wave function. Here a proper account of the Melosh spin rotation and a separation of S and D waves is important especially for excited states. This is in line with our calculations in the momentum space representation [62], using the formalism of [61]. In addition, Refs. [58–60] investigate the dependence on the meson's light front wave function using various potential models.

Many authors have suggested a direct relation of the diffractive coherent amplitude to the collinear gluon distribution of the nucleus. For a useful representation of older data in this context, see [54]. Evidently, in the approach reviewed in this article, no explicit "leading twist" gluon shadowing is present, and there is no direct relation to the DGLAP-evolving collinear nuclear glue. Indeed multiple scatterings of the color dipole generate the leading twist shadowing for *light* quarks [29,30] only. The ALICE data however suggest, that around $x \sim 10^{-3}$, gluon shadowing effects may be important. Recently a reasonable description including gluon shadowing from a DGLAP fit of nuclear partons has been obtained in [45].

Finally, a caveat on our treatment of incoherent diffraction is in order. The use of the completeness relation in the sum over nuclear states, Eq. (27), implies that no additional particles are produced in the final state. Guzey et al. [55] have pointed out that the experimental data can be better described after including nucleon dissociation processes.

4 Low transverse momentum dilepton production in semicentral heavy-ion collisions

We now leave the domain of UPCs, and allow the impact parameter between ions to be small, so that they overlap and collide inelastically [63]. Still, the coherent WW photons must be regarded as partons of the nucleus and can produce dilepton pair even when ions collide and –from the dilepton point of view– give rise to an "underlying event" of high multiplicity, see the diagram Fig. 14.

The $\gamma\gamma$-fusion is of course not the only mode of dilepton production in ultra-relativistic heavy-ion collisions (URHICs). Indeed the investigation of dilepton production in URHICs has a long history as a probe of the hot QCD medium produced in the highly inelastic nuclear collisions [64,65].

There exists a firmly established thermal radiation component from the interacting fireball [66,67]. One distinguishes the low-mass region, i.e. invariant masses $M < 1\,\text{GeV}$, where hadronic radiation dominates. This mass region can be described by the "melting" of the ρ resonance [68]. In the intermediate-mass region, quark-gluon plasma (QGP) radiation dominates [69,70].

Dilepton production is also well established in UPCs [71–73], where no fireball is created. Due to the cutoff on WW-photon transverse momenta this radiation is characterized by very small pair transverse momentum, P_T, and falls off much steeper than for thermal radiation emitted from strongly interacting fireballs. Calculations using WW-fluxes with realistic form factors give a good description of the UPC data [10,74]. The role of WW-photons in peripheral collisions has been recently explored in [75,76].

In Ref. [63] we addressed the interplay of these two processes in peripheral and semi-central heavy-ion collisions, where thermal radiation is suppressed compared to central collisions while the coherent photon emission is still appreciable in the very low-P_T region.

It is interesting to note, that also J/ψ photoproduction in UPCs gives a significant contribution to the low-P_T yields in semi-central collisions at the LHC [77,78], in agreement with the ALICE data [79].

When calculating the cross section for dilepton production via fusion of WW photons, we now omit the "gap survival probability", and allow the impact parameter $\boldsymbol{b}$ to take any value:

$$\frac{d\sigma_{ll}}{d\xi d^2\boldsymbol{b}} = \int d^2\boldsymbol{b}_1 d^2\boldsymbol{b}_2\, \delta^{(2)}(\boldsymbol{b}-\boldsymbol{b}_1-\boldsymbol{b}_2) N(\omega_1,\boldsymbol{b}_1) N(\omega_2,\boldsymbol{b}_2) \times \frac{d\sigma(\gamma\gamma\to l^+l^-;\hat{s})}{d(-\hat{t})}\,, \tag{32}$$

with the phase space element $d\xi = dy_+ dy_- dp_t^2$ where $y_\pm$, p_t and m_l the single-lepton rapidity, transverse momentum and mass, respectively, and

$$\omega_1 = \frac{\sqrt{p_t^2+m_l^2}}{2}\,(e^{y_+}+e^{y_-})\,,$$
$$\omega_2 = \frac{\sqrt{p_t^2+m_l^2}}{2}\,(e^{-y_+}+e^{-y_-})\,,\ \hat{s} = 4\omega_1\omega_2\,. \tag{33}$$

We obtain the dilepton yield in centrality class $\mathcal{C}$ by integrating over an interval $[b_{\min}, b_{\max}]$ associated with the given centrality:

$$\frac{dN_{ll}[\mathcal{C}]}{dM} = \frac{1}{f_{\mathcal{C}}\cdot\sigma_{\text{AA}}^{\text{in}}}\int_{b_{\min}}^{b_{\max}} db \int d\xi\, \delta(M-2\sqrt{\omega_1\omega_2})\,\frac{d\sigma_{ll}}{d\xi db}\Big|_{\text{cuts}}\,,$$

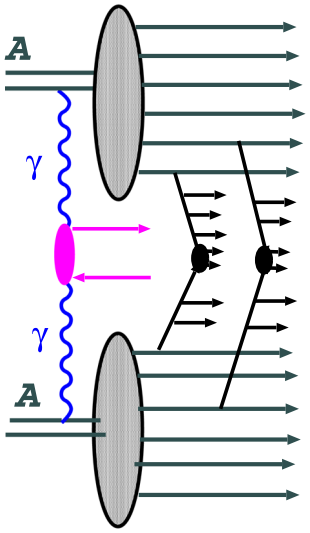

Fig. 14 An inelastic nucleus-nucleus collision including lepton pair production from coherent WW photons of the ions

The fraction of hadronic events in centrality class $\mathcal{C}$

$$f_{\mathcal{C}} = \frac{1}{\sigma_{\text{AA}}^{\text{in}}}\int_{b_{\min}}^{b_{\max}} db\,\frac{d\sigma_{\text{AA}}^{\text{in}}}{db}\,, \tag{34}$$

is used to determine $[b_{\min}, b_{\max}]$ and $\sigma_{\text{AA}}^{\text{in}}$ by using the optical Glauber model,

$$\frac{d\sigma_{\text{AA}}^{\text{in}}}{db} = 2\pi b(1-e^{-\sigma_{\text{NN}}^{\text{in}} T_{\text{AA}}(b)})\,. \tag{35}$$

In Fig. 15 we compare the different dilepton contributions, to data recently released by the STAR collaboration. While thermal radiation (and the hadronic decay "cocktail") dominate the yield for $P_T > 0.2\,\text{GeV}$ at all centralities, while the $\gamma\gamma$-fusion gives rise to the pronounced enhancement at $P_T < 0.15\,\text{GeV}$. Note that a recent transport calculation [81] confirmed that hadronic sources (thermal emission plus cocktail) cannot explain the low-P_T excess observed by STAR in peripheral Au–Au collisions. No photoproduction processes were considered in that study.

Finally, a comment on the transverse momentum spectra is in order. In [63] the P_T distributions were calculated essentially from a convolution of transverse momentum dependent WW fluxes:

$$\frac{d\sigma_{ll}}{d^2\mathbf{P}_T} = \int \frac{d\omega_1}{\omega_1}\frac{d\omega_2}{\omega_2} d^2\mathbf{q}_{1t} d^2\mathbf{q}_{2t}\,\frac{dN(\omega_1,q_{1t}^2)}{d^2\mathbf{q}_{1t}}\,\frac{dN(\omega_2,q_{2t}^2)}{d^2\mathbf{q}_{2t}} \times \delta^{(2)}(\mathbf{q}_{1t}+\mathbf{q}_{2t}-\mathbf{P}_T)\hat{\sigma}(\gamma\gamma\to l^+l^-)\Big|_{\text{cuts}}\,, \tag{36}$$

with

$$\frac{dN(\omega,q_t^2)}{d^2\mathbf{q}_t} = \frac{Z^2\alpha_{EM}}{\pi^2}\,\frac{q_t^2}{[q_t^2+\frac{\omega^2}{\gamma^2}]^2}\,F_{\text{em}}^2(q_t^2+\frac{\omega^2}{\gamma^2}). \tag{37}$$

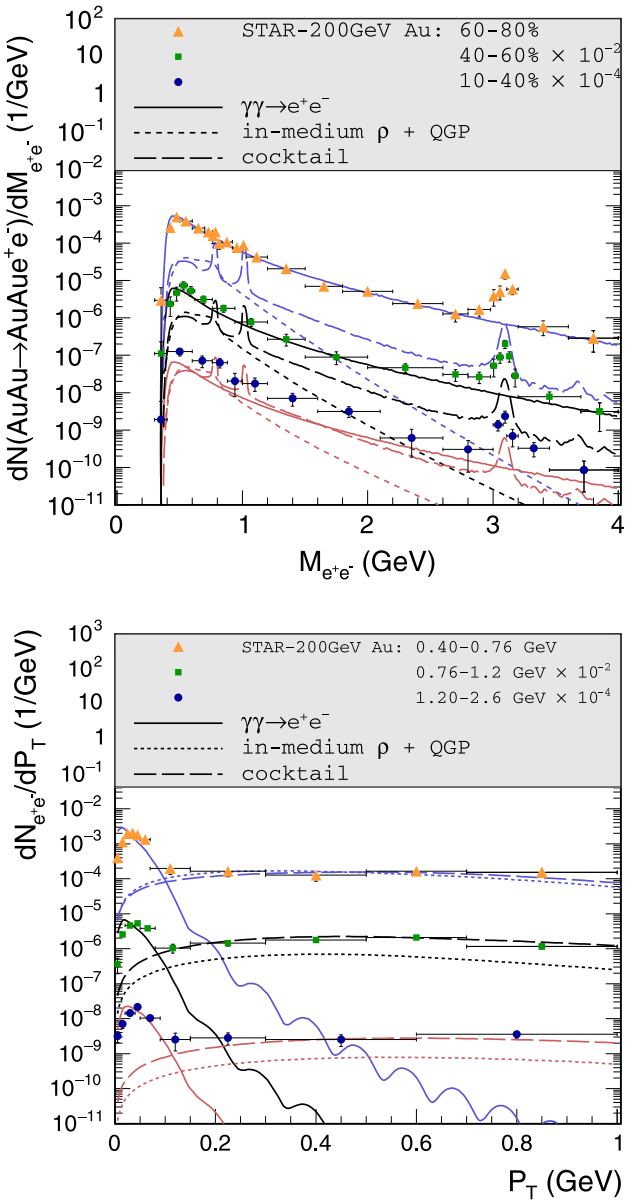

Fig. 15 Upper panel: dielectron invariant-mass spectra for pair-P_T <0.15 GeV in Au + Au($\sqrt{s_{NN}}$=200 GeV) collisions for 3 centrality classes including experimental acceptance cuts (p_t >0.2 GeV, $|\eta_e|$ <1 and $|y_{e^+e^-}|$ <1) for $\gamma\gamma$ fusion (solid lines), thermal radiation (dotted lines) and the hadronic cocktail (dashed lines); Lower panel: P_T spectra of the individual contributions (line styles as in the previous figure) in 3 different mass bins for 60–80% central Au+Au collisions ($\sqrt{s_{NN}}$ = 200 GeV), compared to STAR data [80]

This approach neglects the nontrivial interplay between impact parameters and photon polarizations. In a more refined treatment, one must take into account that the $\gamma\gamma$-system at a fixed impact parameter distance of its sources is prepared as a $\boldsymbol{b}$-dependent mixture of $J_z = 0$ and $J_z = \pm 2$ states. Therefore a full density-matrix approach is called upon. Other potentially important effects such as Sudakov resummation of soft photon emissions and a possible rescattering of dileptons in the plasma have been recently discussed in Ref. [82].

5 Summary

We hope we could give the reader a useful overview on the rich possibilities of photon-induced processes in heavy-ion collisions. Firstly, even when nuclei do not touch each other, they have very large inelastic cross sections. The electromagnetic dissociation cross section is about $\sim$ 200 barn at LHC. Exploiting the high-energy tail of the photon spectrum, photoproduction of J/ψ tells us about interaction of small dipoles with the nuclear medium, potentially about the nuclear gluon distribution. Further data, such as a measurement at central rapidities at $\sqrt{s_{\rm NN}} = 5$ TeV, of transverse momentum distributions as well as production of $\psi(2S)$ would be very interesting. Much additional information on the topic of gluon shadowing is of course expected from a future electron-ion collider [83], where photon virtuality appears as another experimental handle.

The coherent WW photons are also important beyond UPCs–they nicely explain the low-P_T enhancement of dileptons in peripheral and semicentral collisions. The exploration of these processes has just begun.

Finally let us mention some major omissions: firstly, there is the recent observation of light-by-light scattering, see the short review [84]. Secondly, in proton nucleus collisions, heavy ions open a possibility to study high-energy photoproduction on the proton. See e.g. [85] for a proposal to measure the photonic parton distribution in a nucleon.

Acknowledgements This article is a write up of a lecture at the COST workshop/school on Interplay of hard and soft QCD probes for collectivity in heavy-ion collisions at Lund University, Sweden, 25. February - 1. March 2019. I am indebted to Roman Pasechnik for the invitation and to the COST Action CA15213 "Theory of hot matter and relativistic heavy-ion collisions" (THOR) for support.

Data Availability Statement This manuscript has no associated data or the data will not be deposited. [Authors' comment: The datasets generated during and/or analysed during the current study are available from the corresponding author on reasonable request.]

References

1. G. Baur, K. Hencken, D. Trautmann, S. Sadovsky, Y. Kharlov, Phys. Rep. **364**, 359–450 (2002). arXiv:hep-ph/0112211 [hep-ph]
2. C.A. Bertulani, S.R. Klein, J. Nystrand, Ann. Rev. Nucl. Part. Sci. **55**, 271–310 (2005). arXiv:nucl-ex/0502005 [nucl-ex]
3. S. Klein, P. Steinberg, Photonuclear and two-photon interactions at high-energy nuclear colliders. arXiv:2005.01872 [nucl-ex]
4. J.D. Jackson, *Classical Electrodynamics* (Wiley, New York, 1998)
5. M. Kłusek, W. Schäfer, A. Szczurek, Phys. Lett. B **674**, 92–97 (2009). arXiv:0902.1689 [hep-ph]
6. U. Jentschura, V. Serbo, Eur. Phys. J. C **64**, 309–317 (2009). arXiv:0908.3853 [hep-ph]
7. S.R. Klein, J. Nystrand, J. Seger, Y. Gorbunov, J. Butterworth, Comput. Phys. Commun. **212**, 258–268 (2017). arXiv:1607.03838 [hep-ph]
8. J. Bjorken, Phys. Rev. D **47**, 101–113 (1993)
9. G. Baur, L.G. Ferreiro Filho, Nucl. Phys. A **518**, 786–800 (1990)
10. C. Azevedo, V.P. Gonçalves, B.D. Moreira, Eur. Phys. J. C **79**(5), 432 (2019). arXiv:1902.00268 [hep-ph]
11. M. Klusek-Gawenda, M. Ciemala, W. Schäfer, A. Szczurek, Phys. Rev. C **89**(5), 054907 (2014). arXiv:1311.1938 [nucl-th]
12. W. Llope, P. Braun-Munzinger, Phys. Rev. C **41**, 2644–2653 (1990)
13. I. Pshenichnov, Phys. Part. Nucl. **42**, 215–250 (2011)
14. G. Baur, K. Hencken, A. Aste, D. Trautmann, S.R. Klein, Nucl. Phys. A **729**, 787–808 (2003). arXiv:nucl-th/0307031 [nucl-th]
15. R.J. Charity, Phys. Rev. C **82**, 014610 (2010)
16. V. Barone, E. Predazzi, *High-Energy Particle Diffraction* (Springer, Berlin, 2002)
17. I. Ivanov, N. Nikolaev, A. Savin, Phys. Part. Nucl. **37**, 1–85 (2006). arXiv:hep-ph/0501034 [hep-ph]
18. A. Łuszczak, W. Schäfer, Phys. Rev. C **97**(2), 024903 (2018). arXiv:1712.04502 [hep-ph]
19. A. Łuszczak, W. Schäfer, Phys. Rev. C **99**(4), 044905 (2019). arXiv:1901.07989 [hep-ph]
20. B. Abelev et al., ALICE Collaboration. Phys. Lett. B **718**, 1273 (2013). arXiv:1209.3715 [nucl-ex]
21. B.B. Abelev, et al. [ALICE Collaboration], Phys. Rev. Lett. **113**(23), 232504 (2014). arXiv:1406.7819 [nucl-ex]
22. E. Abbas, et al. [ALICE Collaboration], Eur. Phys. J. C **73**(11), 2617 (2013). arXiv:1305.1467 [nucl-ex]
23. V. Khachatryan et al., CMS Collaboration. Phys. Lett. B **772**, 489 (2017). arXiv:1605.06966 [nucl-ex]
24. A. Bursche [LHCb], Nucl. Phys. A **982**, 247–250 (2019)
25. S. Acharya et al., ALICE. Phys. Lett. B **798**, 134926 (2019). arXiv:1904.06272 [nucl-ex]
26. S.R. Klein, J. Nystrand, Phys. Rev. Lett. **92**, 142003 (2004). hep-ph/0311164
27. V.P. Goncalves, M.V.T. Machado, Eur. Phys. J. C **40**, 519 (2005). hep-ph/0501099
28. J.G. Contreras, J.D. Tapia Takaki, Int. J. Mod. Phys. A **30**, 1542012 (2015)
29. N.N. Nikolaev, B. Zakharov, Z. Phys. C **49**, 607–618 (1991)
30. N.N. Nikolaev, Comments Nucl. Part. Phys. **21**(1), 41 (1992)
31. B.Z. Kopeliovich, J. Nemchick, N.N. Nikolaev, B.G. Zakharov, Phys. Lett. B **309**, 179–186 (1993). arXiv:hep-ph/9305225 [hep-ph]
32. J. Nemchik, N.N. Nikolaev, E. Predazzi, B.G. Zakharov, Phys. Lett. B **374**, 199–204 (1996). arXiv:hep-ph/9604419 [hep-ph]
33. H. Kowalski, L. Motyka, G. Watt, Phys. Rev. D **74**, 074016 (2006). arXiv:hep-ph/0606272 [hep-ph]
34. A. Łuszczak, H. Kowalski, Phys. Rev. D **95**(1), 014030 (2017). arXiv:1611.10100 [hep-ph]
35. K.J. Golec-Biernat, M. Wüsthoff, Phys. Rev. D **59**, 014017 (1998). arXiv:hep-ph/9807513 [hep-ph]
36. K. Golec-Biernat, S. Sapeta, JHEP **03**, 102 (2018). arXiv:1711.11360 [hep-ph]
37. E. Iancu, K. Itakura, S. Munier, Phys. Lett. B **590**, 199–208 (2004). arXiv:hep-ph/0310338 [hep-ph]
38. G. Soyez, Phys. Lett. B **655**, 32–38 (2007). arXiv:0705.3672 [hep-ph]
39. W. Schäfer, A. Szczurek, Phys. Rev. D **76**, 094014 (2007). arXiv:0705.2887 [hep-ph]
40. T. Lappi, H. Mantysaari, Phys. Rev. C **87**(3), 032201 (2013). arXiv:1301.4095 [hep-ph]
41. G. Sampaio dos Santos, M.V.T. Machado, J. Phys. G **42**(10), 105001 (2015). arXiv:1411.7918 [hep-ph]
42. V.P. Gonçalves, M.V.T. Machado, B.D. Moreira, F.S. Navarra, G.S. dos Santos, Phys. Rev. D **96**(9), 094027 (2017). arXiv:1710.10070 [hep-ph]
43. Y.P. Xie, X. Chen, Eur. Phys. J. C **76**(6), 316 (2016). arXiv:1602.00937 [hep-ph]
44. J. Cepila, J.G. Contreras, M. Krelina, Phys. Rev. C **97**(2), 024901 (2018). arXiv:1711.01855 [hep-ph]
45. C. Henkels, E.G. de Oliveira, R. Pasechnik, H. Trebien, Phys. Rev. D **102**(1), 014024 (2020). arXiv:2004.00607 [hep-ph]
46. B. Sambasivam, T. Toll, T. Ullrich, Phys. Lett. B **803**, 135277 (2020). arXiv:1910.02899 [hep-ph]
47. G. Chen, Y. Li, K. Tuchin, J.P. Vary, Phys. Rev. C **100**(2), 025208 (2019). arXiv:1811.01782 [nucl-th]
48. J.G. Contreras, Phys. Rev. C **96**(1), 015203 (2017). arXiv:1610.03350 [nucl-ex]
49. J. Cepila, J.G. Contreras, J.D. Tapia Takaki, Phys. Lett. B **766**, 186–191 (2017). arXiv:1608.07559 [hep-ph]
50. M.B.G. Ducati, F. Kopp, M.V.T. Machado, Phys. Rev. D **96**(5), 054001 (2017). arXiv:1708.08546 [hep-ph]
51. M.B. Gay Ducati, F. Kopp, M.V.T. Machado, S. Martins, Phys. Rev. D **94**(9), 094023 (2016). arXiv:1610.06647 [hep-ph]
52. F. Kopp, M.V.T. Machado, Phys. Rev. D **98**, 014010 (2018). arXiv:1806.06701 [hep-ph]
53. A. Cisek, W. Schäfer, A. Szczurek, Phys. Rev. C **86**, 014905 (2012). arXiv:1204.5381 [hep-ph]
54. V. Guzey, E. Kryshen, M. Strikman, M. Zhalov, Phys. Lett. B **726**, 290 (2013). arXiv:1305.1724 [hep-ph]
55. V. Guzey, M. Strikman, M. Zhalov, Phys. Rev. C **99**(1), 015201 (2019). arXiv:1808.00740 [hep-ph]
56. R. Fiore, L. Jenkovszky, V. Libov, M. Machado, Theor. Math. Phys. **182**(1), 141–149 (2015). arXiv:1408.0530 [hep-ph]
57. K.A. Mamo, I. Zahed, Phys. Rev. D **101**(8), 086003 (2020). arXiv:1910.04707 [hep-ph]
58. M. Krelina, J. Nemchik, R. Pasechnik, J. Cepila, Eur. Phys. J. C **79**(2), 154 (2019). arXiv:1812.03001 [hep-ph]
59. J. Cepila, J. Nemchik, M. Krelina, R. Pasechnik, Eur. Phys. J. C **79**(6), 495 (2019). arXiv:1901.02664 [hep-ph]
60. M. Krelina, J. Nemchik, R. Pasechnik, Eur. Phys. J. C **80**(2), 92 (2020). arXiv:1909.12770 [hep-ph]
61. I.P. Ivanov, N.N. Nikolaev, JETP Lett. **69**, 294–299 (1999). arXiv:hep-ph/9901267 [hep-ph]
62. A. Cisek, W. Schäfer, A. Szczurek, JHEP **04**, 159 (2015). arXiv:1405.2253 [hep-ph]
63. M.Kłusek-Gawenda, R. Rapp, W. Schäfer, A. Szczurek, Phys. Lett. B **790**, 339–344 (2019). arXiv:1809.07049 [nucl-th]
64. E.L. Feinberg, Nuovo Cim. A **34**, 391 (1976)
65. E.V. Shuryak, Phys. Lett. B **78**, 150 (1978)
66. I. Tserruya, in *Relativistic Heavy-Ion Physics*, ed. by R. Stock, Landolt Börnstein, New Series (Springer, 2010), vol. I/23A 4-2. arXiv:0903.0415 [nucl-ex]
67. H.J. Specht [for the NA60 Collaboration], AIP Conf. Proc. **1322**, 1 (2010)
68. R. Rapp, G. Chanfray, J. Wambach, Nucl. Phys. A **617**, 472 (1997)
69. R. Rapp, E.V. Shuryak, Phys. Lett. B **473**, 13 (2000)

70. J. Ruppert, C. Gale, T. Renk, P. Lichard, J.I. Kapusta, Phys. Rev. Lett. **100**, 162301 (2008)
71. S. Afanasiev, et al., PHENIX Collaboration. Phys. Lett. B **679**, 321 (2009)
72. E.L. Kryshen for the collaboration [ALICE Collaboration], Photoproduction of heavy vector mesons in ultra-peripheral Pb–Pb collisions. Nucl. Phys. **A967**, 273 (2017)
73. ATLAS Collaboration, ATLAS-CONF-2016-025
74. A. van Hameren, M. Kłusek-Gawenda, A. Szczurek, Phys. Lett. **B776**, 84 (2018)
75. S.R. Klein, Phys. Rev. C **97**, 054903 (2018)
76. W. Zha, L. Ruan, Z. Tang, Z. Xu, S. Yang, Phys. Lett. B **781**, 182 (2018)
77. M. Klusek-Gawenda, A. Szczurek, Phys. Rev. C **93**, 044912 (2016)
78. W. Shi, W. Zha, B. Chen, Phys. Lett. B **777**, 399 (2018)
79. J. Adam, et al., [ALICE Collaboration], Phys. Rev. Lett. **116**, 222301 (2016)
80. J. Adam, et al., STAR Collaboration. Phys. Rev. Lett. **121**, 132301 (2018)
81. T. Song, W. Cassing, P. Moreau, E. Bratkovskaya, Phys. Rev. C **98**, 041901 (2018)
82. S. Klein, A.H. Mueller, B.W. Xiao, F. Yuan, Phys. Rev. Lett. **122**(13), 132301 (2019). arXiv:1811.05519 [hep-ph]
83. A. Accardi, et al., Eur. Phys. J. A **52**(9), 268 (2016). arXiv:1212.1701 [nucl-ex]
84. M. Kłusek-Gawenda, Acta Phys. Polon. B **50**, 1077–1086 (2019)
85. M. Dyndal, A. Glazov, M. Łuszczak, R. Sadykov, Phys. Rev. D **99**(11), 114008 (2019). arXiv:1901.06305 [hep-ph]